Y.Z. Wang, J. Li, S. Zhang, B. Huang, G. Yao, J. Zhang "An RNA Scoring Function for Tertiary Structure Prediction Based on Multi-layer Neural Networks"

Supplementary materials

Table S1. The PDB codes in the training, validation and testing sets, containing 322, 70, and 70 RNAs, respectively.

	PDB codes
Training	2IXZ 2OJ7 1IDV 1R4H 1AFX 1PBM 1RNG 1ZIG 2F87 1HS2 1I46 1I4B 1JZC 1VOP 1FHK 1IK1 1K4A 1K4B 2K65 2KOC 2M1O 2V6W 2Y95 3GVN 4U34 4U35 1Q75 1XWP 2KYE 2LPA 1EKD 1GUC 1JTW 1JWC 1QES 1QET 1XWU 1YFV 2LP9 2MNC 3GLP 402D 4E6B 4JAB 1ATV 1BZ2 1BZ3 1BZU 1FEQ 1J4Y 1KKA 1LUU 1WKS 1YN2 2AWQ 2G1G 2K3Z 2K41 2KPC 2KPD 2KVN 2LA9 2LAC 2LBJ 2M4W 1AJF 1C4L 1MUV 2H49 2IRN 2IRO 2KY2 2QH4 1AJL 1AJT 1ATO 1I3X 1LMV 1LPW 1SLO 2B7G 2MEQ 2MFD 2RLU 1HLX 1MFJ 1RRR 1U2A 2AO5 2O33 2RPK 2RPT 2TOB 17RA 1D0U 1JOX 1JP0 1QWA 2M21 1F9L 1IE1 1IE2 1K2G 1K6G 1K6H 1KD5 1QCU 1TJZ 2G1W 2M12 2HNS 2JSE 2JYM 2K66 2LX1 2M5U 2RRC 4A4S 1BVJ 1JTJ 1K5I 1MFK 1S2F 1S34 1TLR 2ES5 2QH3 2RO2 3PHP 157D 1E4P 1LC6 1MT4 1NC0 1NUV 1SDR 1SY4 1SYZ 280D 2HEM 2LK3 2LV0 2QH2 353D 1EI2 1ELH 1K8S 1KOD 1QC8 2KGP 3CGP 3CGR 1I9X 1QWB 2A43 2L5Z 3CJZ 1A3M 1BYJ 1F6Z 1FQZ 1FYO 1FYP 1Q96 1YSV 2AHT 2IXY 2KXM 2LQZ 2M4Q 2RP0 397D 4NLF 1KPZ 1L2X 1RNA 1YG3 2AP5 2GIP 2LUN 433D 1ANR 1EBQ 1EBS 1NBR 1QD3 1UUD 1UUI 1ZX7 2JWV 2M24 1AJU 1AKX 1EBR 1KP7 1LDZ 1NA2 1RFR 1LVJ 1MFY 1YLG 1YNC 2LDT 1KAJ 1KIS 1KPD 2LI4 2LWK 2RN1 405D 2JXV 2OE5 2XEB 3Q50 1NBK 1R2P 1R7W 1R7Z 1RNK 2EUY 2JLT 2JTP 2KPV 406D 4KYY 1ET4 1FMN 2M57 4PCJ 1E95 1N8X 2FDT 2M23 2TPK 3SJ2 1B36 1F1T 1M5L 1Q8N 2A9L 2KHY 2KTZ 2KU0 3SZX 4E5C 1NTB 2HUA 2AU4 1MWL 2KX8 2L2J 2FEY 2FQN 2O3V 3BNP 1A60 2PN4 3BNL 3LOA 3TD0 3TD1 1BAU 1JU1 1NLC 3BNQ 3MEI 1XJR 1YMO 2KUW 2M8K 2P89 1YKV 4ENB 4OJI 2MHI 3E5C 2KZL 4K27 2LC8 1D4R 2MIY 3FO4 3R4F 3RKF 4PQV 2QUW 2GM0 1KXK 2OIUP 2OIUQ 3LA5 4LX6 3Q3Z 2K4C 4PLX 1P5P 2D1A 2HOJ 2GDI 4FRG 4LVZ 3GX5 4AOB 4B5R 3SUX 2KRL 4FRN 4WFL 2LKR 4QK9 4KQY 4QK8 2QBZ 1U9S 1GID 3D0U 4P8Z 4GMA 3DHS 1Y0Q 4FAW 4R0D
Validation	1F85 2EVY 2VUQ 1OQ0 1EKA 1MWG 2L6I 472D 1BZT 2JSG 2KRZ 2LBL 2GVO 2L8W 1ESY 1XV0 1F5G 2JXQ 2JXS 1JUR 1PJY 2GV4 2L8F 1BGZ 1OW9 2M22 1KKS 2KF0 4JRT 1N53 1DUQ 2R22 1F7H 1XSG 2LJJ 1CSL 1ARJ 1UTS 2L8H 1HWQ 1JO7 1YNG 2KYD 1EHT 1P5N 2D18 2LPT 2L3E 1ZEV 2LUB 1U3K 3SYW 1A51 1CQL 2NOK 2L94 2QEK 2KUU 2QWY 1P5M 2M58 3SLQ 1Y26 4QJH 4JF2 3OWZ 1S9S 3F4G 2HO7 3DIR
Testing	1ESH 1C0O 1ROQ 2V7R 1ATW 165D 1MIS 259D 439D 1KOS 2JR4 2KRP 2LBK 1Z30 2L8U 1DQH 1UUU 1BN0 2U2A 1SZY 1IKD 1OSW 2GV3 2KD8 4A4T 1NEM 2GRW 1RHT 2KEZ 422D 1M82 3CGS 2MIS 1F7F 1TOB 2LDL 28SR 1AQO 1SCL 2K5Z 1F27 2D17 1YNE 1Z31 420D 1T28 2LPS 1T0E 1RAW 3TZR 1TXS 2ZY6 4E48 2O3X 4K31 1XPE 2MTJ 2LU0 4KZ2 4JRC 2MQT 3IVN 4TZX 3D2V 4P5J 4L81 4QLM 2L1F 4GXY 4P9R

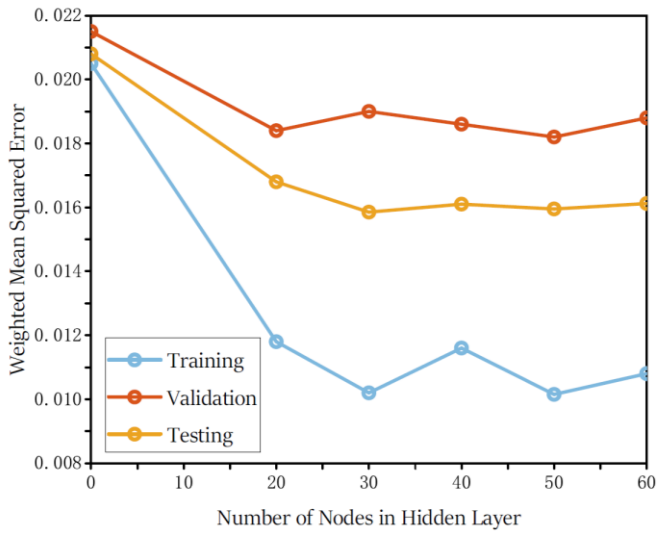

Figure S1. The dependence of error on the number of nodes in the hidden layer, calculated for NET1. The optimal number is chosen to be 30 according to the figure.

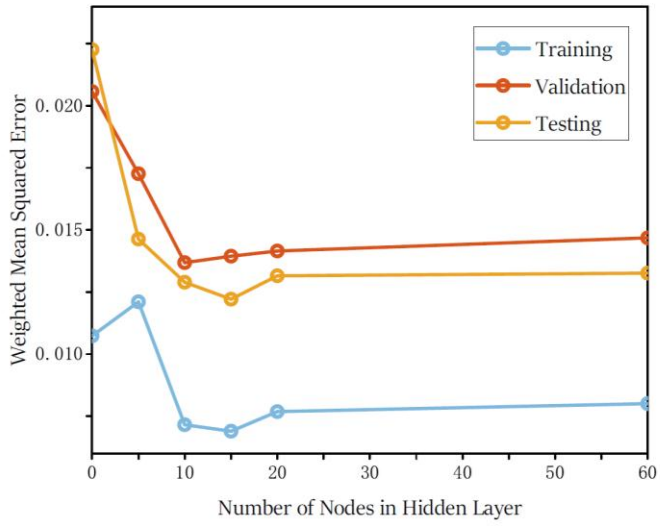

Figure S2. The dependence of error on the number of nodes in the hidden layer, calculated for NET2. The optimal number is chosen to be 10 according to the figure.

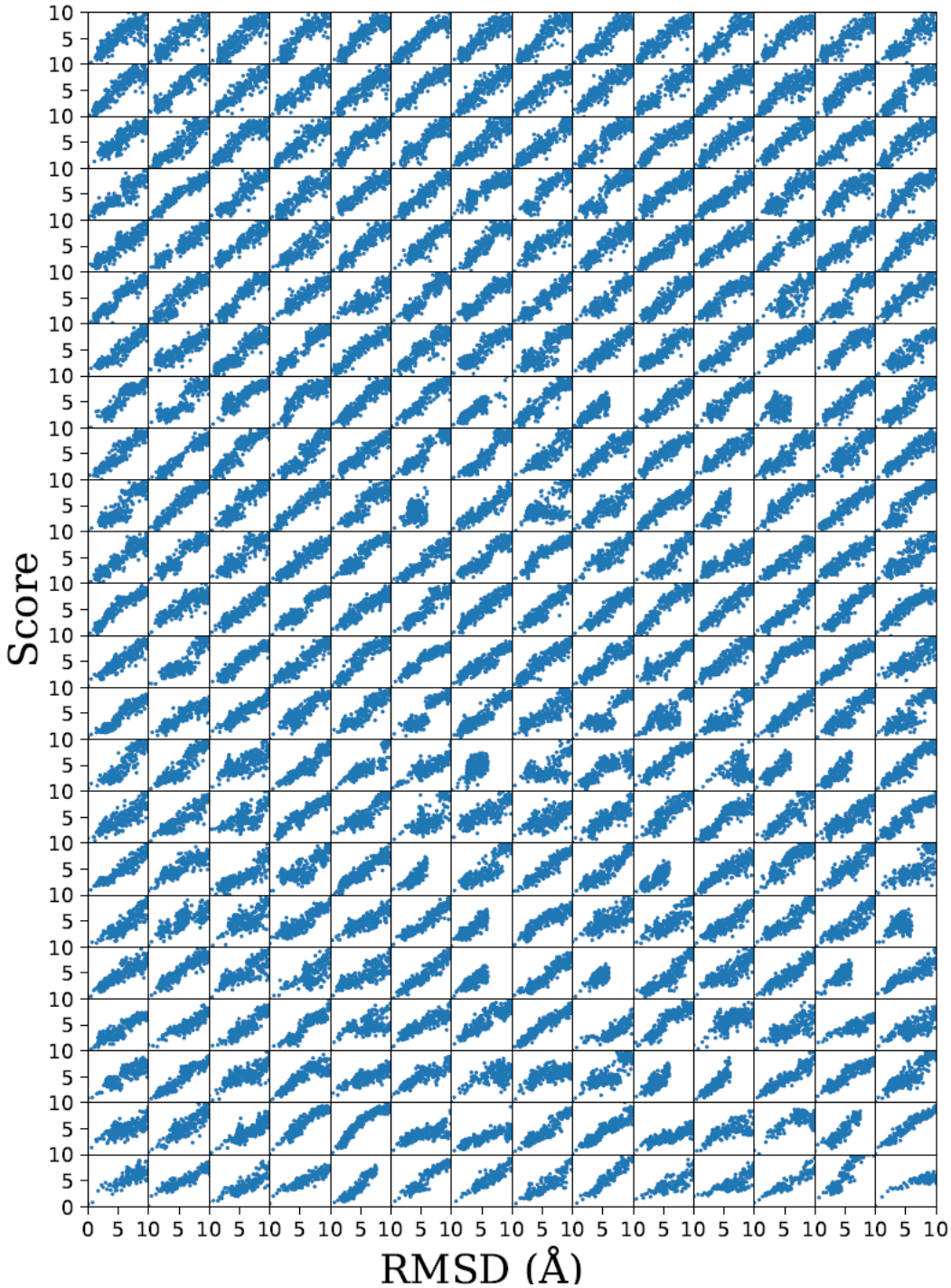

Fig. S3. The correlation between the likeness scores predicted by NET1 and the actual RMSDs, calculated for 322 RNAs in the training set. Each panel corresponds to an RNA and contains 301 structures.

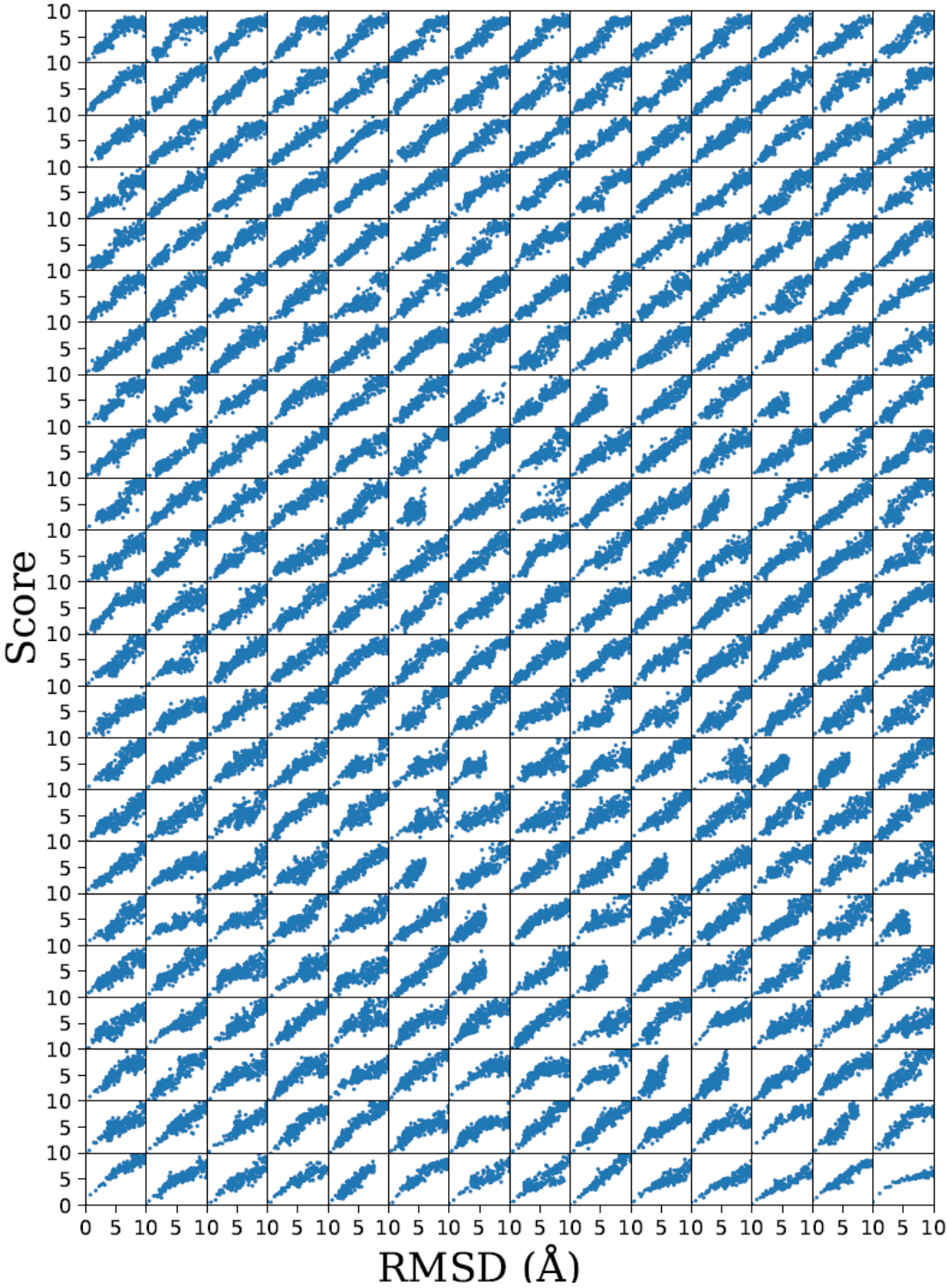

Fig. S4. The correlation between the likeness scores predicted by NET2 and the actual RMSDs, calculated for 322 RNAs in the training set. Each panel corresponds to an RNA and contains 301 structures.

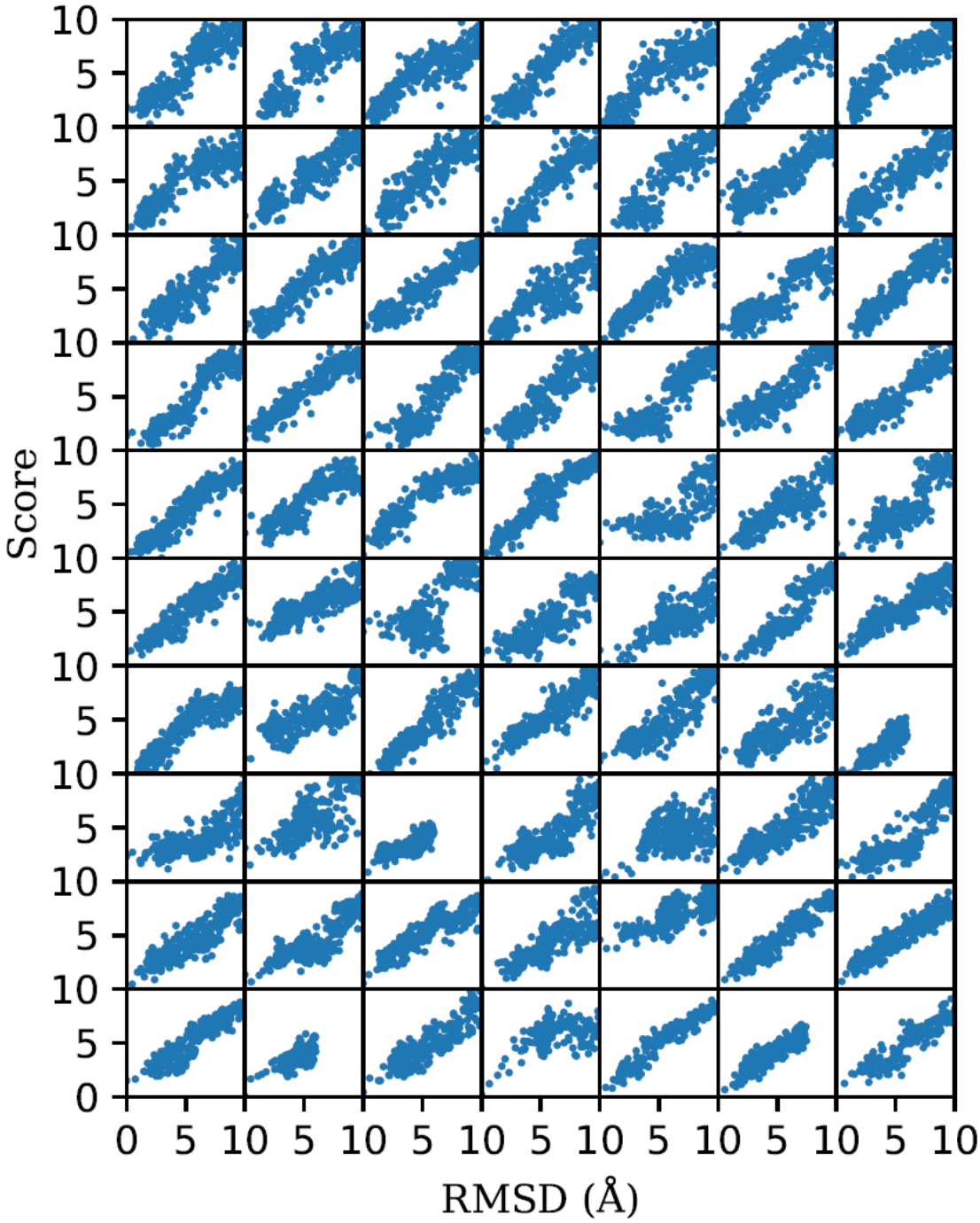

Fig. S5. The correlation between the likeness scores predicted by NET1 and the actual RMSDs, calculated for 70 RNAs in the validation set. Each panel corresponds to an RNA and contains 301 structures.

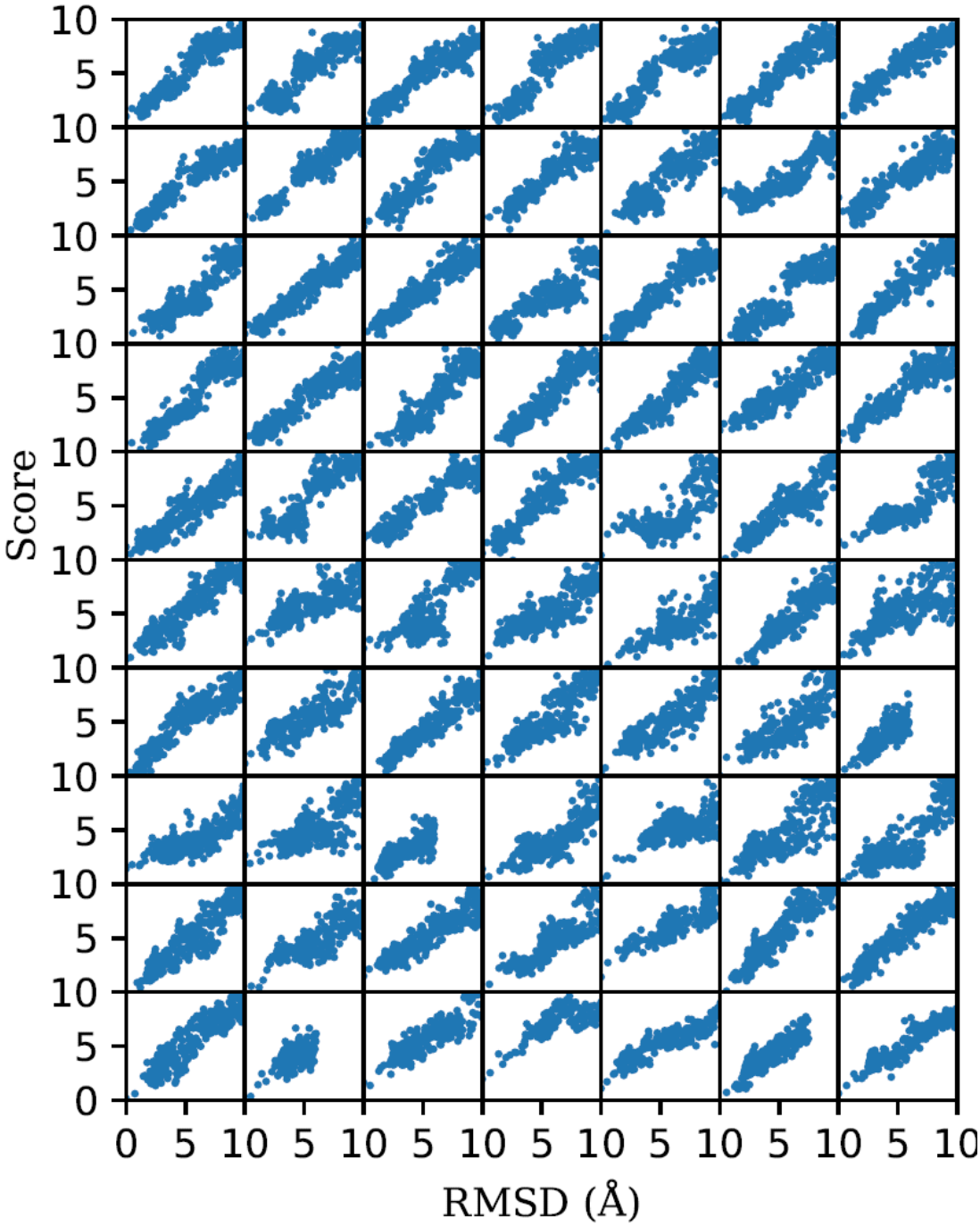

Fig. S6. The correlation between the likeness scores predicted by NET2 and the actual RMSDs, calculated for 70 RNAs in the validation set. Each panel corresponds to an RNA and contains 301 structures.